Applied Physics Express

LETTER • **OPEN ACCESS**

Facile preparation of graphene–graphene oxide liquid cells and their application in liquid-phase STEM imaging of Pt atoms

To cite this article: Masaki Takeguchi *et al* 2024 *Appl. Phys. Express* **17** 085001

OPEN ACCESS

Applied Physics Express 17, 085001 (2024) LETTER

https://doi.org/10.35848/1882-0786/ad63f2

Facile preparation of graphene–graphene oxide liquid cells and their application in liquid-phase STEM imaging of Pt atoms

Masaki Takeguchi[1*], Kazutaka Mitsuishi[2], and Ayako Hashimoto[1,3]

[1]Research Center for Energy and Environmental Materials, National Institute for Materials Science, Japan
[2]Center for Basic Research on Materials, National Institute for Materials Science, Japan
[3]Degree Programs in Pure and Applied Sciences, University of Tsukuba, Japan

*E-mail: TAKEGUCHI.Masaki@nims.go.jp

Received June 26, 2024; revised July 9, 2024; accepted July 16, 2024; published online August 1, 2024

Graphene–graphene oxide (GO) hybrid liquid cells (LCs) for liquid-phase scanning transmission electron microscopy (STEM) were fabricated using a facile method with commercial graphene on a polymethyl methacrylate sheet and GO on a TEM grid. LCs containing Pt nanoparticles (NPs) and pure water were efficiently produced and observed via STEM. Their composition and thickness were characterized by STEM-electron energy-loss spectroscopy. High-resolution (HR) STEM revealed slow-moving Pt NPs' atomic structures and fast-moving single Pt atoms at the LC's thin edges. Minimal damage during HR STEM indicated stable LCs because of their excellent electrical and thermal conductivities and radiolysis species scavenging ability. © 2024 The Author(s). Published on behalf of The Japan Society of Applied Physics by IOP Publishing Ltd

Liquid-phase transmission electron microscopy (LP-TEM) is a powerful tool for observing samples in liquid with high spatial and temporal resolutions.[1–6] A liquid cell (LC) separates the liquid environment of samples from an electron microscope's vacuum using top and bottom membrane windows. The most popular membrane material is a low-stress silicon nitride film deposited on a silicon wafer.[7–9] Using Micro Electro Mechanical Systems (MEMS) fabrication technology, a self-standing silicon nitride membrane window is formed on a silicon chip via back-side etching. Two of the chips are sandwiched and liquid samples are enclosed inside a narrow space between them to complete the LC. Owing to the development of stable and robust LC membranes and MEMS technologies, a set of mass-produced LC chips and dedicated LC TEM holders are commercially available[10] to many researchers, enabling observations of the morphology, structural changes, and chemical reactions of inorganic and biological materials in liquid.[1–14] MEMS-fabricated LCs offer reproducibility, ease of handling, and expandability (e.g., incorporating electrodes and flow systems). However, the membrane thickness (~50 nm) results in resolution deterioration.[3,9,15–17] Another popular type of LC is a graphene LC (GLC), which comprises a pocket containing the liquid and samples between two graphene sheets composed of a single or a few layers.[18–21] GLCs are widely used in academia. Graphene is an ideal LC membrane material as it offers atomic-level thicknesses, low electron scattering characteristics, mechanical flexibility, electrical and thermal conductivity, and chemical stability, enabling atomic-resolution imaging of samples in liquid. However, GLC use is limited because complicated and delicate chemical treatment processes along with technical expertise are needed to prepare GLCs,[22–25] i.e., graphene transfer from CVD-graphene to TEM grids. Furthermore, graphene's hydrophobicity can limit the production yield of liquid pockets.

The present work examines the fabrication of graphene–graphene oxide (GO) LCs using commercially available single-layer graphene sheets and GO-supported TEM grids. Pure water and Pt nanoparticles (NPs) are enclosed in the graphene–GO LC. Characterization was performed using scanning TEM (STEM) and electron energy-loss spectroscopy (EELS) with an aberration-corrected electron microscope (JEM-ARM200F, JEOL Ltd) at 200 kV. The resolution of LP-STEM is better than that of LP-TEM, and aberration-corrected STEM enables imaging of the atomic structures of samples and even single atoms in liquid, whereas scanning speed limits the temporal resolution.[2,17,26] Generally, the basal plane of GO produced by chemical oxidation methods, like the modified Hummers method, predominantly contains epoxy and hydroxyl functional groups,[27–32] resulting in strong water adhesion (i.e., hydrophilicity). This is expected to increase the production yield of liquid sample pockets on GO relative to graphene. Furthermore, GO, similar to graphene, has a radical scavenging effect that migrates radiolysis-induced undesired chemical reactions.[33–35] However, GO is an electrical and thermal insulator, affecting sample and LC stability during TEM. A graphene–GO hybrid sheet exhibits good conductivity,[36] thereby solving this issue. The use of GO for LC (S)TEM has rarely been reported, except for LCs using plasma- or UV-treated graphene,[19] which is thought to be partially oxidized. To the authors' knowledge, LCs with GO for photoelectron spectroscopy[37] and scanning electron microscopy,[38] along with silicon nitride-adhered GO LCs for TEM,[34] have been reported so far. Hence, this study attempts to analyze graphene–GO hybrid LCs with STEM for the first time.

Double layers of GO on holey silicon nitride TEM grids (GNO-2, EMJapan Co. Ltd, Japan) and a single layer of graphene sheet (Trivial Transfer Graphene®, ACS Materials LLC, USA) were used as the GO bottom layer and the graphene top layer of the LCs. The Pt colloidal solution stabilized with tetramethylammonium (4 wt%, Tanaka Kikinzoku Kogyo K. K., Japan) was diluted five times with pure water. Figure 1 shows the graphene–GO LC preparation method. The "Trivial Transfer Graphene®" produced is composed of graphene adhered to a polymethyl methacrylate (PMMA) sheet, with a polymer protection sheet covering it, as shown in Fig. 1(a). The polymer protection sheet was easily removed from the graphene/PMMA sheet by floating

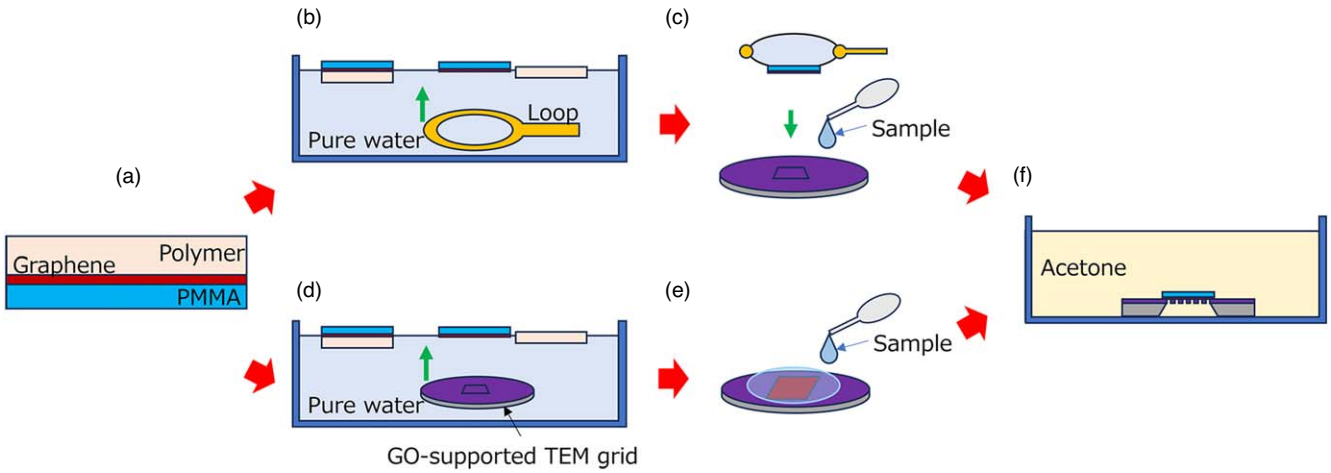

Fig. 1. The graphene–GO LC preparation method: (a) structure of "Trivial Transfer Graphene®"; (b) removal of a polymer protection sheet from graphene/polymethyl methacrylate (PMMA) in pure water, followed by scooping it with a loop; (c) sample drop-casting and placing graphene/PMMA on a GO-supported TEM grid; (d) removal of the polymer protection sheet from graphene/PMMA in pure water, followed by scooping with a GO-supported TEM grid; (e) sample-soaking in a gap between graphene/PMMA and GO on a TEM grid; and (f) PMMA dissolution via acetone treatment.

the sample in pure water for several minutes. Two methods were used to scoop the graphene/PMMA sheet. One involved a loop, as shown in Fig. 1(b). A water droplet with the graphene/PMMA sample was scooped with a loop and placed on a GO-supported TEM grid, as shown in Fig. 1(c). Immediately before this process, a GO-supported TEM grid was illuminated with UV light from an ozone lamp at a power of 4 W for 30–60 s, and a droplet of a sample solution (Pt colloidal solution) was drop-cast onto it. After completely drying the TEM grid, it was immersed in acetone for 30 min to dissolve the PMMA, as shown in Fig. 1(f). It was then rinsed with a mixture of fresh acetone and ethanol. A disadvantage of this method was the difficulty of suspending graphene/PMMA on a water droplet inside the loop, especially when the size of the graphene/PMMA sample was smaller than the loop diameter. Conversely, if the graphene/PMMA size was too large, it covered both the top and bottom sides of the TEM grid. An alternative method involved scooping the graphene/PMMA sample directly with a UV-treated GO-supported TEM grid, as shown in Fig. 1(d), followed by slowly drying it in air. When water on the TEM grid was almost evaporated (not completely dried), a small amount of the Pt colloidal solution was drop-cast onto it to soak into the gap between the GO and graphene, as shown in Fig. 1(e). A drawback of this method was the dilution of the sample solution with the remaining water on the TEM grid.

Figure 2(a) shows an annular dark-field (ADF) STEM image at low magnification, presenting a wide-area view of a graphene–GO membrane suspended across a silicon nitride hole. Enhanced contrast reveals the morphology of the graphene–GO membrane, while the brightness at the silicon nitride region was saturated. Figure 2(b) is a medium-magnification ADF-STEM image, in which large gray areas, as indicated with white arrowheads, and many bright small

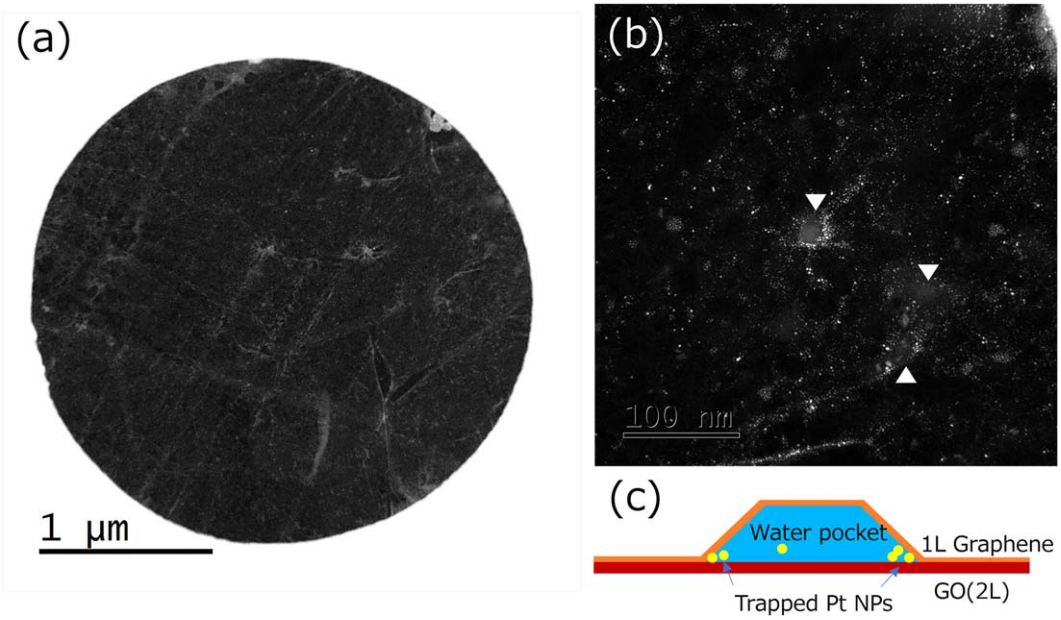

Fig. 2. (a) Annular dark-field (ADF)-STEM wide-area image of a graphene–GO membrane supported on a silicon nitride TEM grid hole; (b) a medium-magnification ADF-STEM image showing large and small graphene–GO LCs; and (c) a schematic of the cross-section of a graphene–GO LC containing water and Pt NPs.

dots are seen. These correspond to liquid pockets (i.e., LCs) and Pt NPs, respectively. Pt NPs appear to decorate the LC's edges and wrinkles of graphene, suggesting the presence of the Pt solution. This is consistent with previous reports of liquids enclosed in dome-shaped pockets and wrinkles of graphene.[19,22] Figure 2(c) illustrates the cross-section of the LC seen at the center of Fig. 2(b), showing that Pt NPs were trapped at the edges of the LC. This trapping occurs because Pt NPs move freely in thicker water but slow down and become immobile in the high-viscosity thin water regions, causing them to accumulate at the edge of the LCs. In Fig. 2(b), small aggregates of Pt NPs also exist, likely corresponding to small LCs. In these thin LCs, Pt NPs are trapped throughout the entire LC.

STEM-EELS elemental mapping was performed to verify the existence of water inside the graphene–GO LCs. Figure 3(a) shows an ADF-STEM image of an LC, while Fig. 3(b) shows EELS elemental maps of carbon (red), oxygen (green), and their mixture, acquired from the green rectangle in Fig. 3(a). The gray center part in the LC contains oxygen and is surrounded by carbon, aligning with the model in Fig. 2(c). It is noted that graphene wrinkles decorated with Pt NPs are composed of oxygen and carbon, albeit with carbon covering a wider region than oxygen, suggesting that water exists inside the graphene wrinkles. The thickness of the LC was estimated to be approximately 30 nm using the log-ratio method, assuming that the inelastic scattering mean free path length for water is 175 nm.[39]

Figure 4(a) is an enlarged ADF-STEM image of the LC in Fig. 3(a). An area inside a green rectangle in Fig. 4(a) was observed by high-resolution (HR) STEM with 1024×1024 pixels at a rate of 19 s/frame. HR STEM movies were recorded using an HD video function of the Gatan Microscopy Suite® (Gatan, USA), with each frame subsequently captured offline. Figure 4(b) is an HR STEM image captured from the movies, in which Pt NPs exist densely along the edge of the LC. The background ADF intensity of the left side of the image is brighter than the right side, indicating a greater amount of water on the left side. As NPs move slowly, which might be caused by the high viscosity of thin water, their atomic structures can be clearly observed, highlighted with pseudo-color for better visibility. Furthermore, small bright dots corresponding to single atoms can be detected, as indicated by white arrows. However, it was difficult to trace the motion of single atoms because they moved faster than the STEM beam scanning speed. Additionally, atoms moving to different heights were defocused and blurred. Notably, there was minimal LC damage during 6 min of HR STEM observations, attributed to their good electrical and thermal conductivities, as

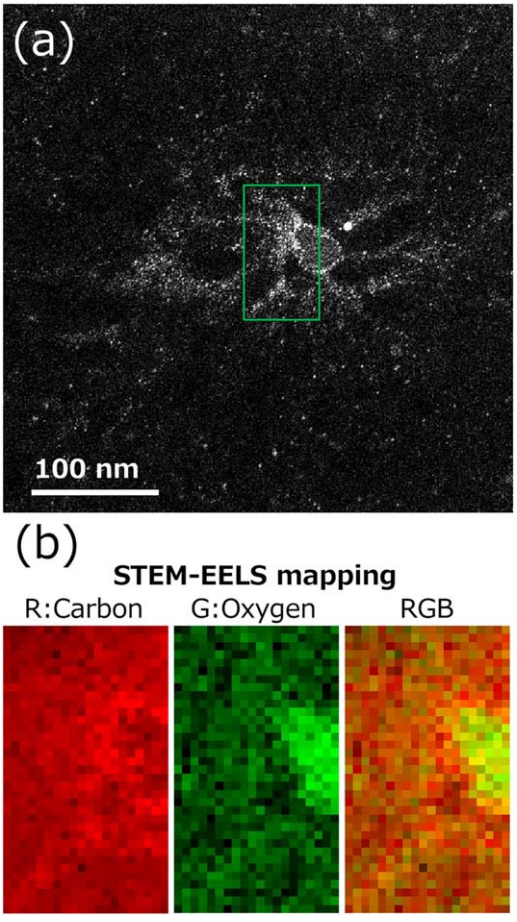

Fig. 3. (a) ADF-STEM image of a graphene–GO LC containing water and Pt NPs. (b) Results of STEM-EELS elemental mapping for a green rectangle area in (a)—R (red) and G (green) correspond to carbon and oxygen elemental maps, respectively. The RGB map is a mixture of carbon and oxygen.

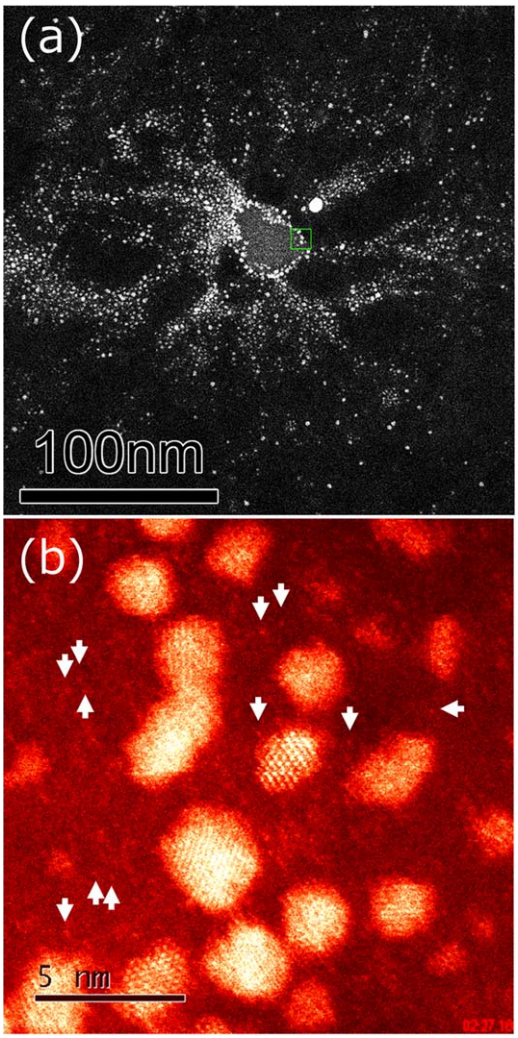

Fig. 4. (a) An enlarged ADF-STEM image of the LC in Fig. 3(a). (b) HR ADF-STEM image of Pt NPs and single atoms (indicated by white arrows) moving in pure water at the edge of the LC. This was a snapshot captured from HR STEM movies.

well as their ability to scavenge radiolysis species of graphene–GO hybrid LCs.

In summary, graphene–GO hybrid LCs for LP (S)TEM were fabricated through a facile method that uses commercially available graphene/PMMA sheets and GO-supported TEM grids. These LCs, applied to STEM imaging of Pt NPs in pure water, exhibited a good production yield, displayed dome pockets, and formed wrinkles decorated with Pt NPs. Their composition and thickness were characterized by STEM-EELS. Atomic structures of Pt NPs moving slowly and Pt single atoms moving fast in water at the thin edge regions of the LCs were observed by HR STEM. Minimal damage during HR STEM observations demonstrated that graphene–GO LCs were stable and robust because of their superior electrical and thermal conductivities, as well as their radiolysis species scavenging ability.

Acknowledgments The authors thank Ms. Y. Kobayashi for helping fabricate graphene–GO LCs, Dr. J. Tang for helpful advice, and Edanz (https://jp.edanz.com/ac) for editing a draft of this manuscript. A part of this work was supported by GteX Program Grant No. JPMJGX23H2, JST, the Innovative Science and Technology Initiative for Security Grant No. JPJ004596, ATLA, Precursory Research for Embryonic Science and Technology Grant No. JPMJPR17S7, JST, and KAKENHI Grant No. 24K08252, JSPS.

ORCID iDs Masaki Takeguchi https://orcid.org/0000-0002-0282-6020 Kazutaka Mitsuishi https://orcid.org/0000-0002-9361-4057 Ayako Hashimoto https://orcid.org/0000-0002-1985-7667

1) F. M. Ross, *Liquid Cell Electron Microscopy* (Cambridge University Press, Cambridge, 2017), 10.1017/9781316337455.
2) N. de Jonge and F. M. Ross, Nat. Nanotechnol. **6**, 695 (2011).
3) N. De Jonge, L. Houben, and R. E. Dunin-Borkowski, Nat. Rev. Matter. **4**, 61 (2019).
4) J. Sung, Y. Bae, H. Park, S. Kang, B. K. Choi, J. Kim, and J. Park, Annu. Rev. Chem. Biomol. Eng. **13**, 167 (2022).
5) S. Pu, C. Gong, and A. W. Robertson, R. Soc. Open Sci. **7**, 191204 (2019).
6) T. Shen, R. Girod, J. Vavra, and V. Tileli, J. Electrochem. Soc. **170**, 056502 (2023).
7) M. J. Williamson, R. M. Tromp, P. M. Vereecken, R. Hull, and F. M. Ross, Nat. Mater. **2**, 532 (2003).
8) X. Li, K. Mitsuishi, and M. Takeguchi, Microscopy **70**, 327 (2021).
9) K. Koo et al., Sci. Adv. **10**, eadj6417 (2024).
10) R. Yang, L. Mei, Y. Fan, Q. Zhang, H. Liao, J. Yang, J. Li, and Z. Zeng, Nat. Protoc. **18**, 555 (2023).
11) U. Mirsaidov, J. P. Patterson, and H. Zheng, MRS Bull. **45**, 704 (2020).
12) D. B. Peckys, E. Macías-Sánchez, and N. de Jonge, MRS Bull. **45**, 754 (2020).
13) M. Takeguchi, X. Li, and K. Mitsuishi, Jpn. J. Appl. Phys. **61**, SD1021 (2022).
14) H. Wu, H. Friedrich, J. P. Patterson, N. A.-J. M. Sommerdijk, and N. de Jonge, Adv. Mater. **26**, 2001582 (2020).
15) N. de Jonge, Ultramicroscopy **187**, 113 (2018).
16) M. Takeguchi, T. Takei, and K. Mitsuishi, Nanomaterials **13**, 2170 (2023).
17) M. Takeguchi, A. Hashimoto, and K. Mitsuishi, Microscopy **73**, 145 (2024).
18) J. Yuk, J. Park, P. Ercius, K. Kim, D. J. Hellebusch, M. F. Crommie, J. Lee, A. Zettl, and A. P. Alivisatos, Science **336**, 61 (2012).
19) J. Park, K. Koo, N. Noh, J. H. Chang, J. Y. Cheong, K. S. Dae, J. S. Park, S. Ji, I. Kim, and J. M. Yuk, ACS Nano **15**, 288 (2021).
20) C. Wang, Q. Qiao, T. Shokuhfar, and R. F. Klie, Adv. Mater. **26**, 3410 (2014).
21) S. M. Ghodsi, C. M. Megaridis, R. Shahbazian-Yassar, and T. Shokuhfar, Small Methods **3**, 1900026 (2019).
22) Y. Sasaki, R. Kitaura, J. M. Yuk, A. Zettl, and H. Shinohara, Chem. Phys. Lett. **650**, 107 (2016).
23) J. Zhang et al., Adv. Mater. **29**, 1700639 (2017).
24) P. M.-G. van Deursen, R. I. Koning, V. Tudor, M. Moradi, J. P. Patterson, A. Kros, N. A.-J. M. Sommerdijk, A. J. Koster, and G. F. Schneider, Adv. Func. Mater. **30**, 1904468 (2020).
25) M. Textor and N. de Jonge, Nano Lett. **13**, 3313 (2018).
26) N. Clark, D. J. Kelly, M. Zhou, Y. Zou, C. W. Myung, D. G. Hopkinson, C. Schran, A. Michaelides, R. Gorbachev, and S. J. Haigh, Nature **609**, 942 (2022).
27) Z. Zhang, H. C. Schniepp, and D. H. Adamson, Carbon **154**, 510 (2019).
28) T. Tsugawa, K. Hatakeyama, J. Matsuda, M. Koinuma, and S. Ida, Bull. Chem. Soc. Jpn. **94**, 2195 (2021).
29) Y. Mulyana, M. Uenuma, Y. Ishikawa, and Y. Uraoka, J. Phys. Chem. C **118**, 27372 (2014).
30) W. Yu, L. Sisi, Y. Haiyana, and L. Jie, RSC Adv. **10**, 15328 (2020).
31) M. Kang et al., Adv. Mater. **33**, 2102991 (2021).
32) J. Fujita et al., Sci. Rep. **13**, 2279 (2023).
33) S. Keskin and N. de Jonge, Nano Lett. **18**, 7435 (2018).
34) H. Cho, M. R. Jones, S. C. Nguyen, M. R. Hauwiller, A. Zettl, and P. AlivisatosA, Nano Lett. **17**, 414 (2017).
35) Z. Lyu, L. Yao, W. Chen, F. C. Kalutantirige, and Q. Chen, Chem. Rev. **123**, 4051 (2023).
36) M. M. Haidari, H. Kim, J. H. Kim, M. Park, H. Lee, and J. S. Choi, Sci. Rep. **10**, 8258 (2020).
37) A. Kolmakov, A. D. Dmitriy, L. J. Cote, J. Huang, M. K. Abyaneh, M. Amati, L. Gregoratti, S. Günther, and M. Kiskinova, Nat. Nanotech. **6**, 651 (2011).
38) Y. Sasaki, S. , Hirayama, and R. Nakao, Microscopy **71**, 175 (2022).
39) S. Keskin, P. Kunnas, and N. de Jonge, Nano Lett. **19**, 4608 (2019).